

# COMPARISON OF UNSTEADY REYNOLDS-AVERAGED NAVIER-STOKES PREDICTION OF SELF-PROPELLED CONTAINER SHIP SQUAT AGAINST EMPIRICAL METHODS AND BENCHMARK DATA

(DOI No: 10.3940/rina.ijme.2020.a2.604)

Z Kok, J T Duffy, S Chai, Australian Maritime College, Australia and Y Jin, Technology Centre for Offshore and Marine Singapore, Singapore

## SUMMARY

The demand to increase port throughput has driven container ships to travel relatively fast in shallow water whilst avoiding grounding and hence, there is need for more accurate high-speed squat predictions. A study has been undertaken to determine the most suitable method to predict container ship squat when travelling at relatively high speeds ( $Fr_h \geq 0.5$ ) in finite water depth ( $1.1 \leq h/T \leq 1.3$ ). The accuracy of two novel self-propelled URANS CFD squat model are compared with that of readily available empirical squat prediction formulae. Comparison of the CFD and empirical predictions with benchmark data demonstrates that for very low water depth ( $h/T < 1.14$ ) and when  $Fr_h < 0.46$ ; Barass II (1979), ICORELS (1980), and Millward's (1992) formulae have the best correlation with benchmark data for all cases investigated. However, at relatively high speeds ( $Fr_h \geq 0.5$ ) which is achievable in deeper waters ( $h/T \geq 1.14$ ), most of the empirical formulae severely underestimated squat (7-49%) whereas the quasi-static CFD model presented has the best correlation. The changes in wave patterns and effective wake fraction with respect to  $h/T$  are also presented.

## NOMENCLATURE

$A_C$	Cross sec. area of canal/channel (m <sup>2</sup> )
$A_E$	Propeller expanded area (m <sup>2</sup> )
$A_O$	Propeller disc area (m <sup>2</sup> )
$A_S$	Immersed midship cross sec. area (m <sup>2</sup> )
AP	Aft perpendicular (m)
$B$	Ship beam (m)
$C_{0.7}$	Propeller chord length at 0.7 radius (m)
$C_B$	Block coefficient
$D_P$	Propeller diameter
FP	Forward perpendicular (m)
$Fr_h$	Froude depth no. ( $Fr_h = U/(gh)^{1/2}$ )
$g$	Gravitational constant (m/s <sup>2</sup> )
$h$	Water depth (m)
$L_{PP}$	Length between perpendiculars (m)
MCTC	Moment to change trim by 1cm (t m)
$n$	Propeller rotation rate (Hz)
$Q$	Propeller torque (Nm)
$T$	Ship draught (m)
$T_P$	Propeller Thrust (N)
TPC	Tonne per centimetre immersion (t/cm)
$P_{0.7}$	Propeller blade pitch at 0.7 radius (m)
$U$	Ship speed (m/s)
UKC	Under-keel clearance (m)
$V_a$	Advance speed (m/s)
$\Delta$	Ship displacement (t)
$\rho$	Density of water (kg/m <sup>3</sup> )
$\nabla$	Ship volumetric displacement (m <sup>3</sup> )

## 1. INTRODUCTION

Due to the highly competitive demands of the shipping industry where larger ships offer more favourable economic returns, it is expected that shipping operators will continue the trend of operating progressively larger ships. Nonetheless, the size growth of next generation ships have and will continue to outpace dredging and harbour expansion projects which are more financially

unfavourable (Gourlay et al., 2015). Therefore, the ship squat phenomenon will continue to pose a severe threat to operational safety in undersized ports.

The severity of ship squat has garnered the attention of various researchers. Pioneering investigations regarding ship squat were conducted by Constantine (1960) where the different squat behaviour for subcritical ( $Fr_h < 1$ ), critical ( $Fr_h = 1$ ) and supercritical ( $Fr_h > 1$ ) vessel speeds were studied. Tuck (1966) introduced a prediction technique for squat prediction in shallow water without lateral restrictions by applying slender-body theory. Continuing his work, Tuck (1973) modified the theory to account for finite channel widths whereas Beck et al. (1974) extended the theory to account for dredged channels. Naghdi and Rubin (1984) further improved Tuck's theory by implementing a nonlinear steady-state solution of the differential equations while Cong and Hsiung (1991) merged the flat ship and thin ship theory to permit the application of the method for transom stern ships.

Besides theoretical methods, prediction techniques based on model scale experiments have also been developed. Model scale experiment squat measurements were presented by Dand and Ferguson (1973) which were then implemented in a semi-empirical prediction technique to predict squat for full form ships with decent accuracy. Empirical formulae which account for different canal cross section parameters were developed by Fuehrer and Römisch (1977). Barrass (1979) presented empirical formulae which account for ship speed, block coefficient and blockage factor. Duffy and Renilson (2000) investigated the effect of propulsion on bulk carrier squat in shallow water where empirical corrections for propulsion effect were presented. A mathematical model to predict unsteady squat and dynamic acceleration effects for a ship traversing in non-uniform water depth was also developed by Duffy (2008). Delefortrie et al.

(2010) presented a mathematical model which accounts for the influence of muddy bottom and propeller action. A semi-empirical model that considers the distribution of the cross-sectional areas of the ship as well as the longitudinal distribution waterline beam of the ship was developed by Lataire et al. (2012). Eloit et al. (2008) developed a Tuck-parameter based mathematical model which incorporated various experimental data of ship, environmental, operational and shipping traffic parameters. Nevertheless, the above work is all based on model scale experiments and thus the scale effect in squat results is not considered.

In recent decades, improved computation power has enabled application of numerical methods to investigate ship squat. A first-order three-dimensional panel method was implemented by Yao and Zou (2010) to predict the shallow water ship squat, which was found to predict sinkage and trim for subcritical and supercritical speeds, but not for trans critical speeds as non-linear effects were neglected. A slender body theory based potential flow alternative was introduced by Zhang et al. (2015) to investigate the hydrodynamic pressure field around a ship travelling in shallow open water, rectangular canal, dredged channel and stepped canal. The method was validated against experimental results in different waterways, but again the method is inappropriate for conditions near the critical speed and above. Gourlay et al. (2016) compared four different potential flow methods; linear 2D, non-linear 1D, double body and a Rankine source code in the estimation of ship squat in confined water for a range of lateral canal widths and water depths. It was shown that the non-linear 1D method provides good estimation of midship sinkage in narrow canals, whereas linear 2D is suitable for wide canals at low speeds and Rankine source method is better for wide canals at high speeds, while the double body method is more consistent for all the tested cases.

The computational fluid dynamics (CFD) method has also been adopted in the study of ship squat as it is able to account for non-linear and viscous effects. Jachowski (2008) used a commercial RANS solver to investigate ship squat in shallow water and showed that the CFD results agree well with empirical methods, experimental observations and wave theory but further investigation is necessary to model the effects of lateral restriction and channel bottom irregularity. Both RANS and hybrid RANS/LES simulations were conducted by Shevchuk et al. (2016) for comparison and to identify the cause of squat intensification at  $h/T < 1.3$  which is often observed in experiments. It was concluded that the union of boundary layers developed both from the ship hull and channel bottom was the cause of the squat intensification. Tezdogan et al. (2016) performed an unsteady RANS simulation of a container ship appended with a fixed propeller in confined water where the resistance and midship sinkage were predicted accurately but trim was excluded from the analysis. RANS simulations conducted by Terziev et al. (2018) showed the significant

effect of a step in channel topography on resistance and squat. Elsherbiny et al. (2020) also demonstrated the relative effect of restrictions imposed by the Suez canal in comparison with a rectangular canal on squat using RANS simulations.

Irrespective of the prediction method applied, there is limited literature regarding investigations on ship squat at relatively high speeds ( $0.5 < Fr_h < 1$ ). Such high speed cases are more common due to the demand to increase vessel speed to increase port throughput. Relevant past studies include the reasonably successful estimation of a bulk carrier squat up to the point of grounding using a Bernoulli equation-based mathematical model for relatively higher water depths (Varyani, 2006). Algie et al. (2018) have also demonstrated the effectiveness of three potential flow and panel code methods in predicting the resistance and squat in transcritical flow within the valid range of the underlying theories. Nonetheless, the mentioned studies do not include self-propulsion effects which has been shown by Lataire et al. (2012) to be significant. In addition, to the authors' knowledge, there are no published numerical studies regarding ship squat with self-propulsion effect in confined water. Therefore, this study aims to develop URANS simulation of container ship squat with self-propulsion effect. Two distinct self-propelled URANS models are compared and assessed. Comparisons are made with respect to the benchmark squat data and existing empirical predictions. Analysis of the wave elevations and novel findings regarding effective wake fractions predicted by a discretised propeller during squat in confined water are also discussed.

## 2. HULL FORM AND CANAL GEOMETRY

The hull form and canal geometry adapted in this study are based on a benchmark case conducted in the Federal Waterways Engineering and Research Institute (BAW) (Mucha et al., 2014). The benchmark case involves the self-propelled Duisburg Test Case (DTC) hull and an asymmetrical canal at a 1:40 scale (refer to Figure 1). The DTC is a 14,000 TEU container ship designed by the Institute of Ship Technology, Ocean Engineering and Transport Systems (ISMT) of the University of Duisburg-Essen for benchmarking purposes. The propeller investigated is the Wageningen B-series 4 bladed propeller (Mucha et al., 2014), operated at model scale self-propulsion point. Principal particulars of the DTC hull and propeller are as shown in Table 1.

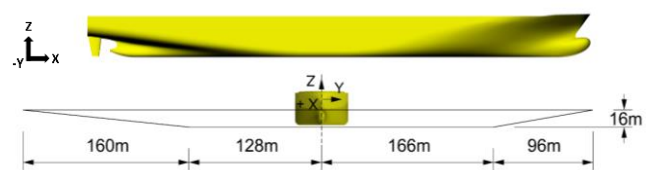


Figure 1: Profile view of the DTC hull (top) and cross section of the asymmetrical canal (bottom).

Table 1: Principal particulars of the hull and propeller.

Principal Particulars	Model Scale (1:40)	Full Scale (1:1)
<b>Ship Particulars</b>		
$L_{PP}$ (m)	8.875	355
$B$ (m)	1.275	51.0
$T$ (m)	0.325	13.0
$\Delta$ (tonnes)	2.618	167,552
$C_B$	0.661	0.661
<b>Propeller Particulars</b>		
$D_P$ (m)	0.223	8.92
Blades	4	4
$P_{0.7}/D_P$	1.275	1.275
$A_E/A_O$	0.55	0.55
$C_{0.7}$ (m)	0.066	2.635

### 3. EXISTING EMPIRICAL PREDICTION METHODS

Several empirical prediction formulae are chosen to assess their accuracy with respect to the benchmark experimental data. Note that the case investigated is container ship squat in a canal. However, most existing empirical formulae are tailored for fuller hull forms ( $C_B > 0.8$ ) where some formulae are only for unrestricted channels whereas others are adapted for restricted channels and canals. In this investigation, formulae adapted for restricted channels and canals as well as those meant for unrestricted channels only are considered for comparison. Similarly, formulae which account for propeller effects and those that do not account for propeller effects are also included for comparison. Hence, the relevant formulae chosen are those of Ankudinov (2009), Barrass (1979), Fuehrer and Römisch (1977), Hooft (1974), Huuska (1976), ICORELS (1980), Millward (1992), and Römisch (1989).

In the Ankudinov (2009) formula, various parameters are accounted for, such as initial trim, propeller parameter and transom factor but a speed restriction of  $Fr_h \leq 0.6$  applies (Briggs, 2009). The Ankudinov (2009) formula is chosen in this study as it is applicable for canals and accounts for propeller effects.

Barrass (1979) formula is developed from regression analysis of more than 600 laboratory and prototype measurements but the nature of the formula is such that it is one of the simplest and user-friendly prediction methods (Serban and Panaitescu, 2015). Note that the formula used in this study is the modified and simplified version known as Barass II (1979).

The formula presented in Fuehrer and Römisch (1977) is based on an energy approach and scale model investigations. This formula is dependent on the critical ship speed which is the speed that cannot be exceeded by typical displacement vessels due to equality between the continuity equation and Bernoulli's Law that introduces unrealistically high drag. The effect of self-propulsion is also accounted for in the prediction. Römisch (1989)

formula is similar to that of Fuehrer and Römisch (1977) where the ship's critical speed is considered (without propeller effect) but that of Römisch (1989) is applicable for restricted channels and canals (PIANC, 1997).

The formula presented in Hooft (1974) is essentially a simplification of Tuck's (1966) theoretical approach while that of Huuska (1976) is a modification of Hooft's formula with additional parameters to account for restricted channels and canals. The ICORELS (1980) formula is also based on Hooft's (1974) simplified formula which is only applicable for unrestricted channels. Note that some authors recommend varying values for  $C_S$  based on the block coefficient when applying the ICORELS (1980) formula. In this investigation, the default value for  $C_S = 2.4$  is applied.

The formula presented in Millward (1992) is also modified from Tuck's (1966) equation but empirical corrections derived from experiments as well as block coefficient have been introduced as factors in the formula. An overview of the application range and properties of all the formulae investigated are tabulated in Table 2 below.

Table 2: Overview of the application range and properties of the formulae used where the symbols U, R and C refer to unrestricted channel, restricted channel and canal respectively.

Formulae	Channel	Constraint					Prop. Effect
		$C_B$	$h/T$	$B/T$	$L_{PP}/B$	$L_{PP}/T$	
Ankudinov (2009)	U, R, C	-	-	-	-	-	✓
Barrass II (1979)	U, R, C	0.50-0.85	1.10-1.40	-	-	-	✗
Fuehrer & Römisch (1977)	U	-	1.19-2.29	-	-	-	✓
Hooft (1974)	U	-	-	-	-	-	✗
Huuska (1976)	U, R, C	0.60-0.80	1.10-2.00	2.19-3.50	5.50-8.50	16.1-20.2	✗
ICORELS (1980)	U	0.60-0.80	1.10-2.00	2.19-3.50	5.50-8.50	16.1-20.2	✗
Millward (1992)	U	0.40-0.85	1.25-6.00	-	-	-	✗
Römisch (1989)	U, R, C	-	1.19-2.25	2.6	8.7	22.9	✗

### 4. COMPUTATION METHOD

URANS simulations are performed in the present study to compare against the experimental benchmark data and the empirical predictions. The commercial CFD solver STAR-CCM+ is used to conduct the computations where the finite volume method of discretisation is applied to resolve the integral form of the incompressible RANS equation.

Table 3 shows the two distinct modelling techniques that were implemented for comparison in the study where one adopts a quasi-static approach (QS) and the other is based on dynamic overset mesh (OV). For the QS model,

the hull is only allowed to surge. The hydrodynamic heave force and pitch moment are measured which in turn are used to calculate the resulting sinkage and trim respectively using the vessel's hydrostatic data. Note that there is no iteration of force and moment balance for the estimated squat to assess the accuracy with minimal run time. The propeller for the QS model is fully-discretised with overset mesh applied to enable rotation relative to the background and forward surge motion together with the hull. In contrast, the OV model has trim and heave motion enabled in addition to surge via the dynamic fluid body interaction (DFBI) module and use of overset mesh over the entire hull. An attempt was made to implement the fully-discretised propeller onto the OV model; however, the resulting run time for the given resources and time-frame of the study is unrealistic. Hence, the propeller model for the OV method is a relatively simpler body-force propulsion virtual disc model.

Table 3: The two distinct CFD modelling techniques implemented in the study.

Technique Name	Quasi-static Model (QS)	Dynamic Overset Model (OV)
Enabled Motion	Hull: Surge Propeller: Rotation & Surge	Hull: Surge, heave & trim Propeller: N/A
Sinkage & Trim Calculation	Hydrostatic data	DFBI Trim & Sinkage
Overset Mesh Region	Propeller	Hull
Propeller Model	Fully-discretised propeller	Body force propulsion virtual disc

The following section discusses the RANS equations and the physics modelling applied. Next, the discretised propeller modelling methodology and results in the form of an open-water propeller simulation are disclosed. Finally, the end of this section then discusses the computation domain set-up, boundary conditions and mesh development for the two self-propelled squat simulation models.

#### 4.1 RANS EQUATIONS

In turbulent flow, field properties become random functions of space and time but this can be resolved by expressing the velocity and pressure fields as the sum of mean and fluctuating components. When the mean and fluctuating components are applied into the incompressible form of the Navier–Stokes equations, the Reynolds-averaged Navier–Stokes equations are effectively derived:

$$\frac{\partial u_i}{\partial x_i} = 0 \quad (1)$$

$$\rho \frac{\partial u_i}{\partial t} + \rho \frac{\partial}{\partial x_j} (U_i U_j) = - \frac{\partial P}{\partial x_i} + \frac{\partial}{\partial x_j} (2\mu S_{ij} - \overline{\rho u_i' u_j'}) \quad (2)$$

$$S_{ij} = \frac{1}{2} \left( \frac{\partial u_i}{\partial x_j} + \frac{\partial u_j}{\partial x_i} \right) \quad (3)$$

In the equations above,  $i$  and  $j$  represents spatial indexes, while  $U_{i(j)}$  and  $P$  are the time-averaged velocity and pressure fields respectively whereas  $\rho$  and  $\mu$  represent the density of the effective flow and viscosity respectively. The term  $S_{ij}$  denotes the mean strain-rate tensor and the term  $\overline{u_i' u_j'}$  denotes the Reynolds stress tensor which is sometimes also expressed as  $\tau_{ij}$ . The Reynolds stress tensor has six components as it is symmetrical. Nonetheless, when the instantaneous properties are decomposed into mean and fluctuating components, three more unknown quantities are introduced into the equations and hence, the Reynolds stress tensor remains unknown. Therefore, to close the system, additional equations (turbulence models) are required. The closure of the equation for this particular investigation is discussed in the following section.

#### 4.2 PHYSICS MODELLING

In this investigation, the RANS equations are closed by implementing the standard k-epsilon (k-ε) turbulence model for both the open-water propeller simulation (discretised propeller modelling) and the two self-propelled squat simulation as Sánchez-Caja et al. (2014) have shown that open-water curves can be predicted accurately using k-ε model and similarly, sinkage prediction is also reported to be insensitive to turbulence models (Deng et al., 2014). It should also be noted that for both simulations, the segregated flow model is implemented and the convection terms of the RANS equations are discretised using a second order upwind scheme.

The domain for the open-water propeller simulation only has a single (water) phase. In contrast, the domain for the two self-propelled simulation has both gas (air) and liquid (water) phases. According to Deng et al. (2014), the sinkage experienced by a hull as it advances is dependent on the free surface position and this is especially true for confined water conditions. Therefore, for the self-propelled squat simulations, modelling of the free surface has been taken into account in this investigation by applying the volume of fluid (VOF) method. The second order discretization scheme is applied to obtain sharp interfaces between the gas and liquid phases.

Motion for the open-water propeller simulation is made possible by means of simple body rotation for the propeller. However, for the two self-propelled squat simulations, the dynamic fluid body interaction (DFBI) module is enabled to allow hull motions. The body-force propulsion virtual disc model is applied for the OV model.

For all simulations, the implicit unsteady approach is adopted. Hence, the time-step ( $\Delta t$ ) is determined based on the Courant number (CFL) as expressed in Equation 4 below where  $\Delta l$  is mesh length parallel to the flow and  $U$  is the mesh flow speed. In the determination of the time-step, the CFL number is set to 1 i.e. flow moves about 1

cell size per time-step for the region with the finest mesh (hull bottom). A second order temporal discretisation scheme is used.

$$\Delta t = \frac{CFL \times \Delta l}{U} \quad (4)$$

### 4.3 DISCRETISED PROPELLER MODELLING

Prior to designing the self-propelled QS model with a discretised propeller, the discretised propeller modelling technique itself must be validated against benchmark data first. The validation is to be done by conducting an open-water propeller simulation for the discretised propeller and then comparing the computed open-water curves predicted against the benchmark data.

In this investigation, the open-water propeller simulation is modelled based on the cavitation tunnel method with constant loading (ITTC, 2014) as it is relatively simple to model. The propeller rotation speed,  $n$  is fixed at 800 RPM throughout the open-water propeller simulations to ensure that the required rotation speed for self-propulsion of the DTC hull at the highest speed in this investigation ( $0.56 Fr_h$ ) can be validated.

The open water propeller simulation was set-up in a domain of length  $25D_p$  and square cross-section of  $10 D_p \times 10 D_p$ . The velocity inlet flow speed is varied while the bottom, top and both sides of the domain are also assigned as velocity inlets but with zero velocity. Figure 2 illustrates the dimensions and boundary condition setting of the domain.

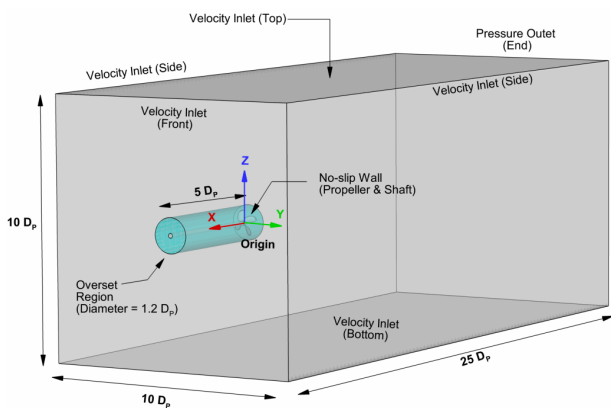


Figure 2: The open water propeller simulation domain design and boundary conditions.

The computational grids were generated using the STAR-CCM+ built-in hexahedral trimmed cell mesher and surface remesher. Overset mesh was implemented to enable the rotation of the propeller in the domain. The prism layer mesher is applied to achieve  $y^+ > 30$  for the propeller blade surface. Care is taken to provide additional mesh refinement on the propeller blade surface and slow cell growth rate is implemented to

ensure smooth transition of mesh size between the fine blade mesh and coarser background mesh. The set-up consists of 1,303,639 cells where 607,091 are dedicated to the overset region. Figure 3 shows the domain and propeller mesh.

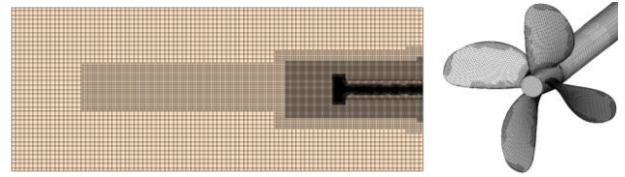


Figure 3: Side view of the open water propeller simulation set-up (left) and perspective view of the propeller mesh (right).

In order to produce the open water curves, the advance ratio,  $J$ , thrust coefficient,  $K_T$ , torque coefficient,  $K_Q$ , and propeller efficiency,  $\eta_o$  are calculated using the below equations respectively.

$$J = \frac{V_A}{nD_p} \quad (5)$$

$$K_T = \frac{T_p}{\rho n^2 D_p^4} \quad (6)$$

$$K_Q = \frac{Q}{\rho n^2 D_p^5} \quad (7)$$

$$\eta_o = \frac{JK_T}{2\pi K_Q} \quad (8)$$

These non-dimensional values are plotted and compared against that of the experimental data (Barnitsas et al., 1981) as shown in Figure 4. As observed, the open water curves produced by the discretised propeller model correlates strongly with the experimental data. Slight discrepancies are observed when  $J > 0.9$  particularly for  $K_Q$  (approximately 17% difference). However, operation at such high  $J$  is also unrealistic. Hence, the discretised propeller modelled is feasible for application in the QS model.

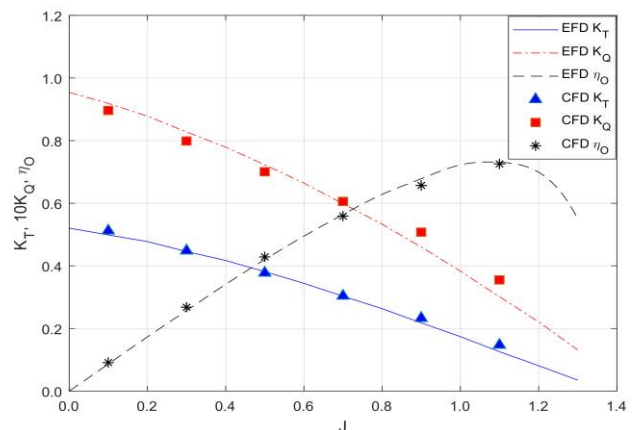


Figure 4: Open water propeller curve results from CFD and EFD (Barnitsas et al., 1981).

#### 4.4 COMPUTATIONAL DOMAIN, BOUNDARY CONDITIONS AND MESH OF SELF-PROPELLED SQUAT SIMULATION

The computational domain for both QS and OV models are designed based on the benchmark case set-up discussed in earlier where the cross-section of the domain is identical to that shown in Figure 1 whereas the position of the outlet, inlet and top boundaries can be seen in Figure 5.

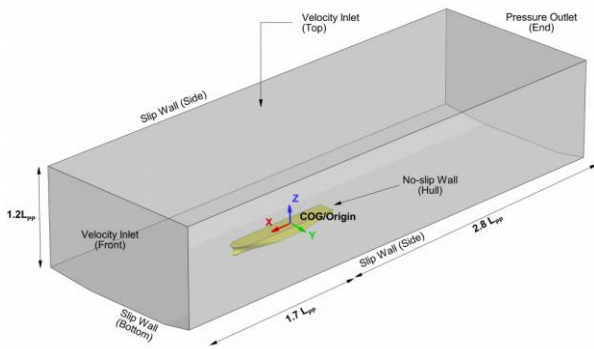


Figure 5: The domain dimensions and boundary conditions applied for the two squat models.

The set-up of the simulation is such that the domain moves forward together with the hull to more realistically model motion of a hull in a stationary body of water. Therefore, the inlet generates zero velocity flat waves and backflow is prevented by the pressure outlet. In addition, VOF wave damping of length  $1.13 L_{PP}$  is applied to the inlet and outlet to prevent unrealistic wave reflections from the said boundaries. The top of the domain is set as a zero velocity inlet. The surfaces of the hull and propeller are assigned as no-slip walls to capture

the boundary layers that develop as the hull advances. Slip wall condition is applied on the two side walls and bottom of the domain to prevent the development of a velocity profile due to the domain's motion. However, the slip condition will mean that the velocity profile development on the bottom due to the moving hull will not be captured too. Nevertheless, Deng et al. (2014) have shown that squat is insensitive to the near wall treatments applied to the bottom of the domain and thus, the slip wall condition will be of no concern.

Similar to the open-water propeller simulation, the STAR-CCM+ built-in hexahedral trimmed cell mesher and surface remesher are used to generate the computational grids for both squat models with reference to CD-Adapco (2014) recommendations for virtual towing tank simulations. To accurately capture the developed boundary layers, Kelvin wave pattern and the underkeel flow characteristics, attention is given to provide refined meshing to the hull surfaces, free surface region and the narrow underkeel clearance respectively. Smooth mesh size transition between regions of highly refined mesh and the coarser mesh regions is made possible by applying slow cell growth rate. The prism layer mesher is used to model the turbulent boundary layer with  $y^+$  value of 30 or above. For the QS model, the overset mesh is implemented on the propeller to enable superposed rotation where the resultant thrust and torque are transferred to the hull. Mesh setting and refinement for the propeller are identical to that implemented in the open-water propeller simulation. For the OV model, the overset mesh is applied on the entire hull instead to enable heave and trim motion relative to the background (refer to Figure 6). As suggested by CD-Adapco (2014), a distance of at least 4 grids is maintained between the overset region surface and hull surface (or propeller surface in the case of QS model).

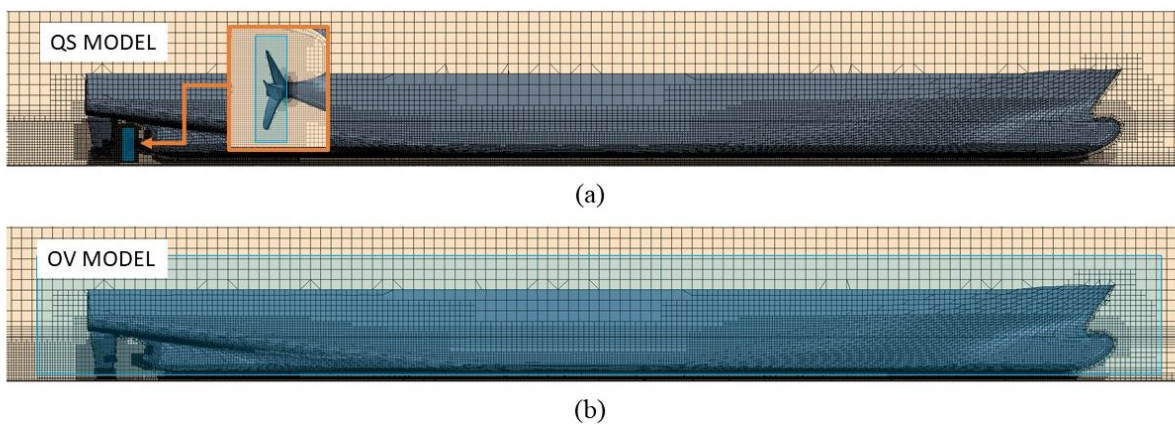


Figure 6: Profile view of the hull mesh for the QS model with overset mesh (in blue) applied onto the discretised propeller (a) and the hull mesh for the OV model with overset mesh applied over the entire hull (b).

## 5. VERIFICATION AND VALIDATION OF NUMERICAL COMPUTATION METHOD

This section discusses the verification and validation procedure and results for the self-propelled squat simulation. Note that the QS model is used for the verification and validation studies as the QS model is more stable and reliable at higher speeds compared to the OV method (refer to Section 7 for further discussion). The method applied is based on the triplets method discussed by Wilson et al. (2001) and Stern et al. (2001). The method is similar to that adapted by Jin et al. (2016). The verification and validation of the self-propelled squat simulation are conducted for the case of  $h/T = 1.23$  with  $n = 430$  RPM which is approximated to yield ship speed of  $0.5 Fr_h$ .

### 5.1 VERIFICATION AND NUMERICAL UNCERTAINTY

As described in the procedure discussed by Wilson et al. (2001) and Stern et al. (2001), the numerical uncertainty  $U_{SN}$  is approximated as the combination of iterative convergence uncertainty  $U_I$ , grid spacing uncertainty  $U_G$  and time step uncertainty  $U_T$  as shown in Equation 9. However, the iterative uncertainty for ship motion response simulations in Star-CCM+ URANS solver is less than 0.2% and hence  $U_I$  is neglected in this study (Tezdogan et al., 2015).

$$U_{SN}^2 = U_I^2 + U_G^2 + U_T^2 \quad (9)$$

Triple solutions are each obtained for both the grid and time step uncertainty convergence study where the grid spacing uncertainty analysis is conducted with the smallest time-step while the time-step uncertainty study is conducted with the finest mesh setting. In the grid spacing uncertainty study, a refinement ratio of  $r_G = \sqrt{2}$  is applied to the background while the mesh of the hull was kept consistent to maintain the accuracy of the surface modelling. Details of the mesh count for the grid spacing uncertainty study are shown in Table 4.

In regards to the time-step uncertainty study, the time-step is determined using Equation 4 as mentioned earlier and the refinement ratio for time-step  $r_T$  is 2.

Table 4: Mesh count details for the grid spacing uncertainty study.

Mesh Configuration	Total Mesh
Coarse (3)	1,493,484
Medium (2)	2,686,488
Fine (1)	3,988,335

Summarised in Table 5 and Table 6 are the outcomes of the grid spacing and time-step uncertainty analysis. In the verification analysis, the AP and FP sinkage as well as the ship speed are monitored because the ship speed is dependent on the mesh quality and  $n$  of the discretised

propeller. It can be seen that the ship speed varies with the mesh quality and hence the resultant AP and FP sinkage also vary. For the grid spacing uncertainty study, monotonic convergence (MC) is achieved for ship speed while oscillatory convergence (OC) is achieved for both AP and FP sinkage but the uncertainty for all three variables are less than 3%.

Table 5: Grid spacing uncertainty analysis summary where MC is monotonic convergence and OC is oscillatory convergence.

Variable	Solutions ( $\times 10^{-3}$ )			Conv. Ratio	$U_G$ (% $S_1$ )
	Coarse ( $S_3$ )	Medium ( $S_2$ )	Fine ( $S_1$ )		
Ship Speed (m/s)	963	975	985	0.75 (MC)	2.74
AP Sinkage (m)	2.86	3.04	3.01	-0.15 (OC)	2.89
FP Sinkage (m)	1.52	1.65	1.62	-0.26 (OC)	3.94

Table 6: Time-step uncertainty analysis summary where MC is monotonic convergence and OC is oscillatory convergence.

Variable	Solutions ( $\times 10^{-3}$ )			Conv. Ratio	$U_T$ (% $S_1$ )
	Long ( $S_3$ )	Medium ( $S_2$ )	Short ( $S_1$ )		
Ship Speed (m/s)	947	971	985	0.56 (MC)	2.67
AP Sinkage (m)	2.60	2.88	3.01	0.46 (MC)	10.4
FP Sinkage (m)	1.55	1.59	1.62	0.65 (MC)	3.04

Similarly, for the time-step uncertainty study, the ship speed and therefore the AP and FP sinkage vary with time-step. Monotonic convergence is achieved for all three variables where the uncertainty is between 2-10%. The numerical uncertainties are deemed to be acceptable.

### 5.2 VALIDATION AGAINST MODEL TEST DATA

Validation against the benchmark data is conducted by comparing the comparison error  $E$ , with the validation uncertainty  $U_V$ .  $U_V$  is the combination of numerical uncertainty,  $U_{SN}$  and experimental uncertainty  $U_D$  as given below:

$$U_V = \sqrt{U_{SN}^2 + U_D^2} \quad (10)$$

Next, the comparison error,  $E$ , is calculated as the difference between the experimental data,  $D$ , and simulation data,  $S$ . The numerical results are considered to be validated if  $E$  is less significant than  $U_V$ :

$$E = D - S \quad (11)$$

The results of the validation study are summarised in Table 7. It should be noted that that  $U_D$  is not provided in the literature and as a compromise, a value of 5% is assumed. The estimated  $E$  for AP sinkage is smaller than  $U_V$  and is therefore validated. However, the estimated  $E$  for FP sinkage is 9% larger than  $U_V$  and is thus not validated. Regardless, it should be noted that the percentage of  $E$  appears large due to the fact that the FP sinkage has a relatively small value where small differences will result in large percentage differences. Also, considering that the value of  $U_D$  is estimated, it is reasonable to state that the current numerical method yields results with reasonable accuracy and is feasible for further investigations.

Table 7: Validation results.

Sinkage	$U_{SN}$ (%)	$U_D$ (%)	$U_V$ (%)	$E$ (%)
AP	10.79	5.00	11.9	-7.17
FP	4.95	5.00	7.03	16.7

### 6. BENCHMARK CASES

Having verified and validated the QS model, the same mesh configuration is adapted to the OV model resulting in mesh size of 3,799,211 where 1,076,902 grids are overset meshes. Further systematic study can then be conducted to compare and assess the accuracy of the empirical formulae and the two CFD model predictions against the benchmark experimental data. The comparison is conducted at three even-keel draughts, each with varying speed ranges according to the benchmark data as tabulated in Table 8.

Table 8: Summary of benchmark case data for the investigation.

Full scale $T$ (m)	$h/T$	Ship Speed		$Fr_h$
		FS (knots)	MS (m/s)	
13.0	1.23	5.06 – 13.56	0.41 – 1.10	0.21 – 0.56
14.0	1.14	4.83 – 13.23	0.39 – 1.08	0.20 – 0.54
14.5	1.10	2.42 – 12.20	0.20 – 0.99	0.10 – 0.50

### 7. RESULTS

#### 7.1 COMPARISON BETWEEN METHODS

The results of the empirical formulae predictions and self-propelled simulations along with the experimental data for  $h/T = 1.10$ ,  $h/T = 1.14$  and  $h/T = 1.23$  are as depicted in Figure 7, Figure 8 and Figure 9, respectively. Note that most of the empirical formulae investigated only output the maximum sinkage. Since the hull trims stern down, the empirical predictions should be taken as squat by the AP (stern) and compared against the experimental AP sinkage.

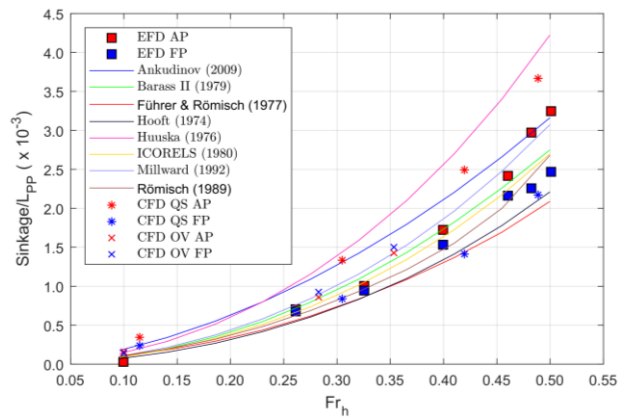


Figure 7: Comparison of the AP sinkage (positive downward) predicted by the empirical formulae and self-propelled CFD simulation against experimental data for  $h/T = 1.10$ .

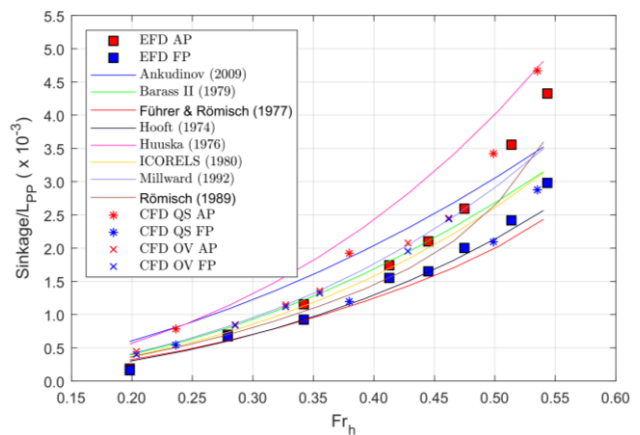


Figure 8: Comparison of the AP sinkage (positive downward) predicted by the empirical formulae and self-propelled CFD simulation against experimental data for  $h/T = 1.14$ .

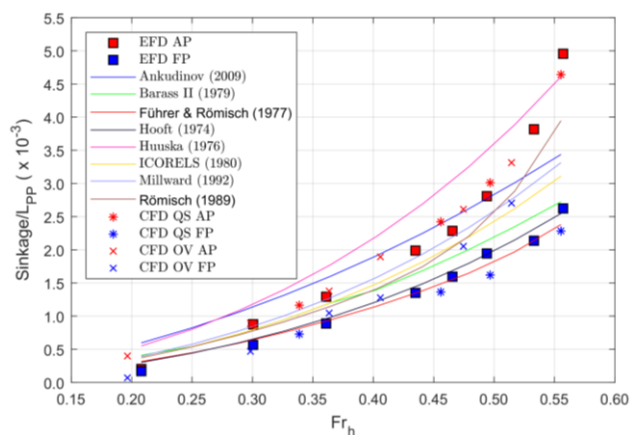


Figure 9: Comparison of the AP sinkage (positive downward) predicted by the empirical formulae and self-propelled CFD simulation against experimental data for  $h/T = 1.23$ .

As expected, observations on the results of all three  $h/T$  cases in Figure 7, Figure 8 and Figure 9 show that the empirical formulae predictions can vary significantly which agrees with findings of past similar studies (Elsherbiny et al. 2020; Terziev et al. 2018). For this particular study, the formula presented in Huuska (1976) outputs the largest predictions whereas that of Fuehrer and Römisch (1977) outputs the smallest predictions. It is of interest to note that the Römisch (1989) and Millward (1992) predictions produce reasonably good trendlines throughout the cases investigated even though Römisch’s formula does not account for self-propulsion whereas Millward’s formula does not account for both lateral restrictions and self-propulsion. In contrast, despite the holistic nature of the Ankudinov (2009) formulae, the outcome of the predictions’ accuracy is marginal.

In regards to the CFD predictions, the OV model exhibits stability issues as evident by the lack of data points at higher speeds. The DFBI module for heave and trim applied for the OV model requires sufficient grids (space) in the UKC for the hull to gradually trim and sink in an oscillatory manner until it reaches a dynamic equilibrium irrespective of the ramp time allocated. Convergence cannot be achieved if the initial oscillatory motion causes the hull to contact the bottom boundary.

The higher the speed of travel, the greater the initial oscillatory motion becomes and therefore the highest speed that the OV methods can achieve convergence reduces as the UKC decreases (shallower water). In contrast, the QS model which is fixed from heaving and trimming does not have such issues and is able to converge for all cases investigated.

When comparing the accuracy of each empirical formulae and CFD predictions relative to the benchmark results, it is found that the performance of each prediction differs from one  $h/T$  case to another. Table 9 summarises the most suitable prediction methods for each  $h/T$  case. It can be observed that the predictions using the ICORELS (1980) and Millward (1992) methods are one of the very few which are suitable for all three  $h/T$  cases, provided that  $Fr_h < 0.46$ . It is noted that almost all the empirical formulae are no longer suitable at higher speeds ( $Fr_h > 0.5$ ) where the relative difference to the benchmark results can vary from 7-49%. Similarly, the OV model is able to yield reasonable AP sinkage predictions for all three  $h/T$  cases but is unable to converge at higher speeds. Furthermore, observations on the FP sinkage prediction from the OV model suggest there are inaccuracies in the trim prediction and the midship sinkage too. Thus, the OV model is not recommended in Table 9.

Instead, the QS model predictions are the most favourable at relatively high speeds where  $Fr_h > 0.5$  as seen in the case for  $h/T = 1.14$  and  $h/T = 1.23$  while also having good correlation with the benchmark data for both AP and FP sinkage. Thus, the QS model is recommended for prediction of high speed container ship

squat where  $Fr_h > 0.5$  which is achievable in  $h/T \geq 1.14$  while the Barass II (1979), ICORELS (1980) and Millward (1992) methods are recommended for very shallow cases where  $h/T < 1.14$  and  $Fr_h < 0.46$ .

Table 9: Most suitable prediction methods for each  $h/T$  case.

Case	Most Suitable Prediction	Overall Difference w.r.t. Benchmark Data (%)	
		Average	Standard Dev.
$h/T = 1.10$	Barass II ( $Fr_h < 0.46$ )	-3.64	6.95
	ICORELS ( $Fr_h < 0.46$ )	-5.35	7.01
	Millward	1.31	3.99
$h/T = 1.14$	Barass II ( $Fr_h < 0.47$ )	-1.55	6.62
	ICORELS ( $Fr_h < 0.47$ )	-3.36	6.59
	Millward ( $Fr_h < 0.47$ )	0.86	4.80
	Römisch ( $Fr_h < 0.50$ )	-4.36	5.30
	CFD QS ( $Fr_h \geq 0.50$ )	11.7	2.15
$h/T = 1.23$	Ankudinov ( $Fr_h < 0.50$ )	1.95	6.44
	ICORELS ( $Fr_h < 0.47$ )	-5.55	6.84
	Millward ( $Fr_h < 0.47$ )	-3.43	5.90
	Römisch ( $Fr_h < 0.52$ )	-4.25	3.92
	CFD QS	1.86	3.52

Regardless, the QS model is undoubtedly computationally intensive as it requires 129-143 hours of simulation time to reach convergence when computed on 156 processors with an average of 27 seconds of CPU time per time-step. Future work of this study will explore various CFD modelling alternatives to determine the most suitable model for systematic investigations such as the feasibility of virtual disc propeller for the QS model instead.

## 7.2 ANALYSIS OF THE WAVE ELEVATION

Having established that the QS model is the more reliable CFD method, analysis of the wave elevation and wake characteristics are made based on the QS model results to better understand the flow physics.

Figure 10 compares the wave elevations of the three  $h/T$  cases with similar  $Fr_h$ . It is observable that the wave elevations for the deeper draught condition ( $h/T = 1.10$ ) is significantly greater than that of the shallower draught ( $h/T = 1.23$ ) which is expected since the case with the deeper draught (larger displacement) will require more energy to move forwards. Subsequently, the greater energy input to the system will form larger waves. It is of interest to note the formation of transverse bow waves in the  $h/T = 1.14$  & 1.10 case which signifies near trans-critical flow (Constantine, 1960). For the  $h/T = 1.23$  case, the asymmetric nature of the flow due to the asymmetric canal is well observed. For all three cases, the free surface depression at midship which causes squat is also clearly seen.

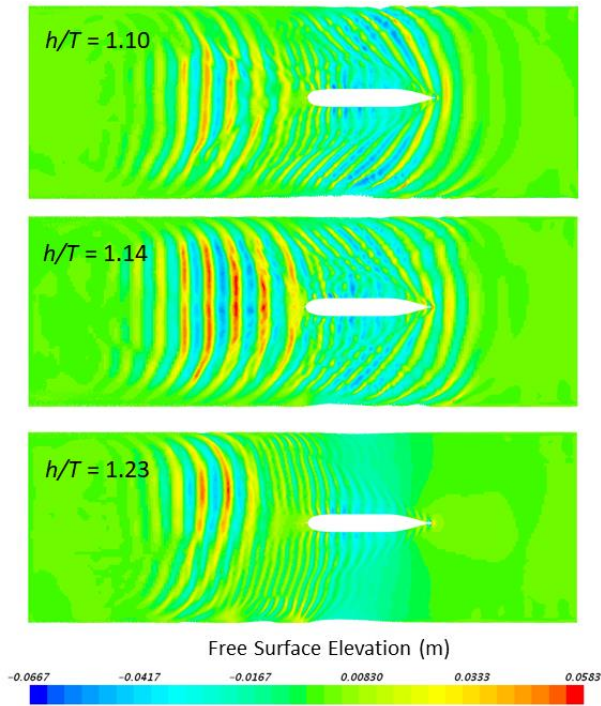


Figure 10: Comparison of free surface elevations for the three  $h/T$  cases at approximately  $0.5 Fr_h$ . The asymmetric waves are manifestations of the asymmetric canal.

### 7.3 INFLUENCE OF WATER DEPTH-TO-DRAUGHT RATIO ON WAKE FRACTION

The profile view of the stern region wake fraction depicted on the left side of Figure 11 shows that as the

$h/T$  increases, the wake on the bottom of the canal immediately aft of the propeller decreases significantly. Further plots of the effective wake fraction on the right side of Figure 11 clearly shows that the wake from the keel gradually connects with the canal bottom as the  $h/T$  decreases. Consequently, the flow velocity at the bottom half of the propeller decreases. The wake from the stern of the hull above the propeller is also greater when  $h/T$  decreases. Overall, the effective wake fraction becomes greater when  $h/T$  decreases. Table 10 shows that the mean effective wake fraction for the speeds investigated increase when  $h/T$  decreases. However, the effective wake fraction is expected to be greater than presented in this study if the hull is allowed to sink and trim freely.

Table 10: Results for mean effective wake fraction,  $w$ .

$h/T$	$Fr_h$	$w$
1.10	0.115	0.343
	0.305	0.333
	0.420	0.312
	0.489	0.338
	<b>Average</b>	<b>0.320</b>
1.14	0.236	0.354
	0.380	0.272
	0.499	0.260
	0.535	0.268
	<b>Average</b>	<b>0.272</b>
1.23	0.339	0.133
	0.456	0.206
	0.497	0.246
	0.540	0.215
	<b>Average</b>	<b>0.204</b>

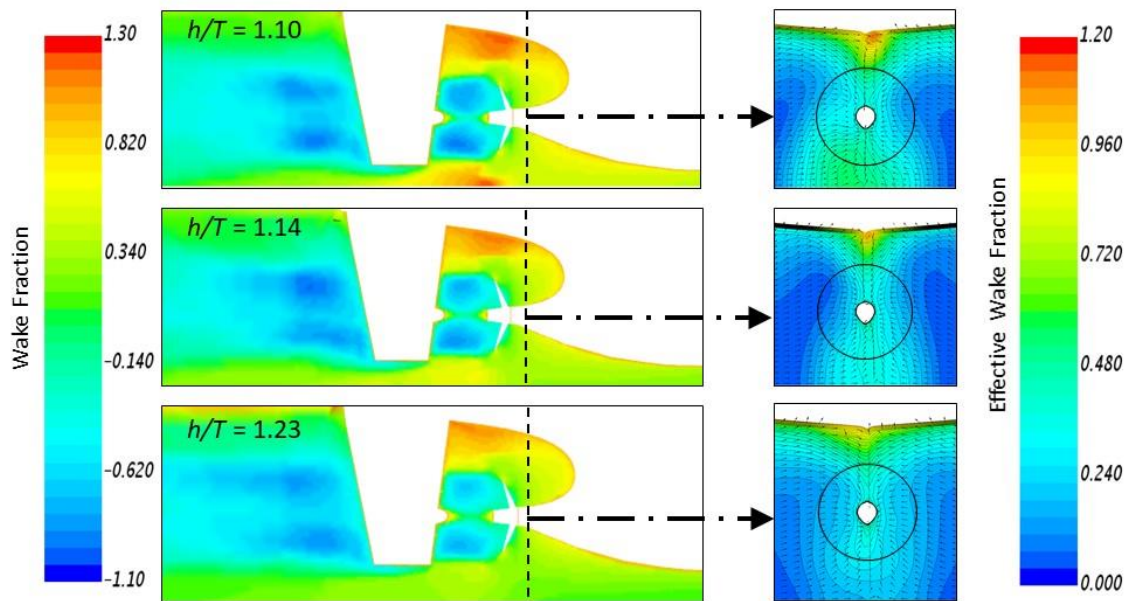


Figure 11: Profile view of the wake fraction at the stern region for the three  $h/T$  cases at approximately  $0.5 Fr_h$  (left) with a corresponding cross-sectional view of the effective wake fraction ahead of the propeller as indicated by the dotted cut (right, not to scale to the left profile view).

## 8. CONCLUDING REMARKS

The demand for increased port throughput has driven the need for container ships to travel relatively fast in shallow water and hence, better squat prediction accuracy is required to optimise the ship speed whilst avoiding grounding. Hence, an investigation has been conducted to assess the accuracy of two novel self-propelled CFD squat models in comparison to several empirical formulae for the prediction of container ship squat at relatively high speeds ( $Fr_h \geq 0.5$ ). The predictions are compared to benchmark model scale experimental squat data on the DTC hull in one of the PreSquat workshops conducted in BAW (Mucha et al., 2014).

This study demonstrates that the accuracy of each method with respect to the benchmark data can vary depending on the  $h/T$  and that the squat predicted can also differ significantly between methods. In regards to the empirical formulae investigated, it is observed that the ICORELS (1980) and Millward (1992) methods are one of the very few which are suitable for all three  $h/T$  cases, provided that  $Fr_h < 0.46$ . Most of the empirical formulae are unable to accurately predict squat for  $Fr_h > 0.5$ . On the contrary, the QS model presented in this study demonstrates excellent accuracy for  $Fr_h > 0.5$ .

Hence, for relatively lower speeds ( $Fr_h < 0.41$ ) in very shallow cases where  $h/T < 1.14$ , empirical predictions by Barass II (1979), ICORELS (1980) and Millward (1992) are recommended whereas for higher speeds ( $Fr_h \geq 0.5$ ) which is achievable in deeper waters of  $h/T \geq 1.14$ , the QS model predictions is preferable.

Analysis of the QS model computations demonstrate that the wave elevation profile changes with  $h/T$ . Decrease in  $h/T$  results in larger waves and greater ease in achieving near trans-critical flow which is manifested as large transverse bow waves. Observations on the wake characteristics show that the effective wake fraction increases when  $h/T$  decreases due to the increased wake from the hull stern and the gradual merging of the keel wake with the canal bottom.

The authors believe that the CFD model developed in this study can be further optimised for further systematic investigations. Future work of this study will focus on various CFD modelling techniques to determine the most suitable model.

## 9. ACKNOWLEDGEMENTS

The authors acknowledge the funding and resources provided by NCMEH Australian Maritime College, University of Tasmania and the Tasmanian Partnership for Advanced Computing for the HPC for performing the computations.

## 10. REFERENCES

1. ALGIE, C., GOURLAY, T., LAZAUSKAS, L. & RAVEN, H. (2018) *Application of potential flow methods to fast displacement ships at transcritical speeds in shallow water*. Applied Ocean Research, 71, 11-19.
2. BARNITSAS, M. M., RAY, D. & KINLEY, P. (1981) *KT, KQ and efficiency curves for the wageningen b-series propellers*. University of Michigan.
3. BARRASS, C. (1979) *The phenomena of ship squat*. International Shipbuilding Progress, 26.
4. BECK, R. F., NEWMAN, J. N. & TUCK, E. O. 1974. *Hydrodynamic forces on ships in dredged channels*. Journal of Ship Research, 19(03), 166-171.
5. BRIGGS, M. J. (2009) *Ankudinov Ship Squat Predictions-Part 1: Theory, Parameters, and Fortran Programs*. Coastal and Hydraulics Engineering Technical Note ERDC/CHL CHETN-IX-19, US Army Engineer Research & Development Centre, Vicksburg, MS.
6. CD-ADAPCO (2014) *User guide STAR-CCM+ Version 9.0.6*.
7. CONG, L. & HSIUNG, C. (1991) *Computing Wave Resistance, Wave Profile, Sinkage And Trim Of Transom Stern Ships*. Proceedings of the Third International Conference on Computer Aided Design, Manufacture and Operation in the Marine and Offshore Industries (CADMO 91), Key Biscayne, pp. 99-112.
8. CONSTANTINE, T. (1960) *On the movement of ships in restricted waterways*. Journal of Fluid Mechanics, 9, 247-256.
9. DAND, I. & FERGUSON, A. (1973) *The squat of full ships in shallow water*. National Physical Lab Teddington (England) Ship Div.
10. DELEFORTRIE, G., VANTORRE, M., ELOOT, K., VERWILLIGEN, J. & LATAIRE, E. (2010) *Squat prediction in muddy navigation areas*. Ocean Engineering, 37, 1464-1476.
11. DENG, G., GUILMINEAU, E., LEROYER, A., QUEUTEY, P., VISONNEAU, M. & WACKERS, J. (2014) *Simulation of container ship in shallow water at model scale and full scale*. Proceedings of the 3rd National CFD Workshop for Ship and Offshore Engineering (25-26 July 2014, China).
12. DUFFY, J. & RENILSON, M. (2000) *An investigation into the effect of propulsion on ship squat*. Oceanic Engineering International, 4, 1-12.
13. DUFFY, J. T. (2008) *Modelling of ship-bank interaction and ship squat for ship-handling simulation*. PhD Thesis, University of Tasmania, Launceston, Australia.
14. ELOOT, K., VERWILLIGEN, J. & VANTORRE, M. (2008) *An overview of squat measurements for container ships in restricted water*. International

- conference on safety and operations in canals and waterways SOCW, 15-16.
15. ELSHERBINY, K., TERZIEV, M., TEZDOGAN, T., INCECIK, A. & KOTB, M. (2020) *Numerical and experimental study on hydrodynamic performance of ships advancing through different canals*. Ocean Engineering, 195, 106696.
  16. FUEHRER, M. & RÖMISCH, K. (1977) *Effects of modern ship traffic on islands and ocean waterways and their structures*. 24th International Navigation Congress, PIANC, 236-244. Leningrad, USSR.
  17. GOURLAY, T., LATAIRE, E. & DELEFORTRIE, G. (2016) *Application of potential flow methods to ship squat in different canal widths*. 4th MASHCON. Bundesanstalt für Wasserbau, 146-155.
  18. GOURLAY, T. P., HA, J. H., MUCHA, P. & ULICZKA, K. (2015) *Sinkage and trim of modern container ships in shallow water*. Australasian Coasts & Ports Conference 2015: 22nd Australasian Coastal and Ocean Engineering Conference and the 15th Australasian Port and Harbour Conference, Engineers Australia and IPENZ, 344.
  19. HOOFT, J. (1974) *The behaviour of a ship in head waves at restricted water depths*. International Shipbuilding Progress, 21, 367-390.
  20. HUUSKA, O. (1976) *On the evaluation of underkeel clearances in Finnish waterways*. Helsinki University of Technology, Ship Hydrodynamics Laboratory, Otaniemi, Report, 9.
  21. ITTC (2014) *Open Water Test*. Recommended Procedures and Guidelines, 1-11.
  22. JACHOWSKI, J. (2008) *Assessment of ship squat in shallow water using CFD*. Archives of Civil and Mechanical Engineering, 8, 27-36.
  23. JIN, Y., DUFFY, J., CHAI, S., CHIN, C. & BOSE, N. (2016) *URANS study of scale effects on hydrodynamic manoeuvring coefficients of KVLCC2*. Ocean Engineering, 118, 93-106.
  24. LATAIRE, E., VANTORRE, M. & DELEFORTRIE, G. (2012) *A prediction method for squat in restricted and unrestricted rectangular fairways*. Ocean Engineering, 55, 71-80.
  25. MILLWARD, A. (1992) *Comparison of the Theoretical and Empirical Prediction of Squat in Shallow Water*. International Shipbuilding Progress, 39, 69-78.
  26. MUCHA, P., EL MOCTAR, O. & BÖTTNER, C.-U. (2014) *PreSquat—Workshop on numerical prediction of ship squat in restricted waters*. Ship Technology Research, 61, 162-165.
  27. NAGHDI, P. & RUBIN, M. (1984) *On the squat of a ship*. Journal of ship research, 28, 107-117.
  28. PIANC, A. C. (1997) *A Guide for Design*. Final Report of the Joint Working Group PIANC–IAPH, Supplement to Bulletin np, 95.
  29. SÁNCHEZ-CAJA, A., GONZÁLEZ-ADALID, J., PÉREZ-SOBRINO, M. & SIPILÁ, T. (2014) *Scale effects on tip loaded propeller performance using a RANSE solver*. Ocean Engineering, 88, 607-617.
  30. SERBAN, P. S. & PANAITESCU, V. N. (2015) *Comparison Between Formulas Of Maximum Ship Squat*. Mircea cel Batran Naval Academy Scientific Bulletin, 19(1), 105-111.
  31. SHEVCHUK, I., BÖTTNER, C.-U. & KORNEV, N. (2016) *Numerical Analysis of the Flow in the Gap Between the Ship Hull and the Fairway Bottom in Extremely Shallow Water*. 4th MASHCON-International Conference on Ship Manoeuvring in Shallow and Confined Water with Special Focus on Ship Bottom Interaction, 37-42.
  32. STERN, F., WILSON, R. V., COLEMAN, H. W. & PATERSON, E. G. (2001) *Comprehensive approach to verification and validation of CFD simulations—part 1: methodology and procedures*. Journal of fluids engineering, 123, 793-802.
  33. TERZIEV, M., TEZDOGAN, T., OGUZ, E., GOURLAY, T., DEMIREL, Y. K. & INCECIK, A. (2018) *Numerical investigation of the behaviour and performance of ships advancing through restricted shallow waters*. Journal of Fluids and Structures, 76, 185-215.
  34. TEZDOGAN, T., DEMIREL, Y. K., KELLETT, P., KHORASANCHI, M., INCECIK, A. & TURAN, O. (2015) *Full-scale unsteady RANS CFD simulations of ship behaviour and performance in head seas due to slow steaming*. Ocean Engineering, 97, 186-206.
  35. TEZDOGAN, T., INCECIK, A. & TURAN, O. (2016) *A numerical investigation of the squat and resistance of ships advancing through a canal using CFD*. Journal of Marine Science and Technology, 21, 86-101.
  36. TUCK, E. (1966) *Shallow-water flows past slender bodies*. Journal of Fluid Mechanics, 26, 81-95.
  37. TUCK, E. (1973) *Sinkage and trim in shallow water of finite width*. Schiffstechnik, 14.
  38. VARYANI, K. (2006) *Squat effects on high speed craft in restricted waterways*. Ocean engineering, 33, 365-381.
  39. WILSON, R. V., STERN, F., COLEMAN, H. W. & PATERSON, E. G. (2001) *Comprehensive approach to verification and validation of CFD simulations—Part 2: Application for RANS simulation of a cargo/container ship*. Journal of fluids engineering, 123, 803-810.
  40. YAO, J.-X. & ZOU, Z.-J. (2010) *Calculation of ship squat in restricted waterways by using a 3D panel method*. Journal of Hydrodynamics, Ser. B, 22, 489-494.
  41. ZHANG, Z.-H., DENG, H. & WANG, C. (2015) *Analytical models of hydrodynamic pressure field causing by a moving ship in restricted waterways*. Ocean Engineering, 108, 563-570.

APPENDIX

Formulae Name	Formulae
Ankudinov (2009)	$S_{max} = L_{PP}(S_{mid} \pm 0.5Trim)$ where – is for bow squat, + is for stern squat  $S_{mid} = (1 + K_p^S) P_{Hu} P_{Frh} P_{+h/T} P_{Ch1}$ $K_p^S = 0.15$ for single propeller $K_p^S = 0.13$ for twin propellers  $P_{Hu} = 1.7C_B \left( \frac{BT}{L_{PP}^2} \right) + 0.004C_B^2$ $P_{Frh} = Fr_h^{(1.8+0.4Fr_h)}$ $P_{+h/T} = 1 + \frac{0.35}{(h/T)^2}$  $P_{Ch1} = 1$ for unrestricted channel $P_{Ch1} = 1 + 10S_h - 1.5(1 + S_h)\sqrt{S_h}$ for restricted/canal  $S_h = C_B \left( \frac{A_s/A_c}{h/T} \right) \left( \frac{h_T}{h} \right)$ $Trim = 1.7P_{Hu} P_{Frh} P_{h/T} K_{Tr} P_{Ch2}$ $P_{h/T} = 1 - e^{-\left[ \frac{2.5(1-h/T)}{Fr_h} \right]}$ $K_{Tr} = C_B^{Tr} - (0.15K_p^S + K_p^T) - (K_B^T - K_{Tr}^T - K_{T1}^T)$ $nTr = 2 + 0.8 \frac{P_{Ch1}}{C_B}$  $K_p^T = 0.15$ for single propeller $K_p^T = 0.20$ for twin propellers $K_B^T = 0.1$ for bulbous bow $K_B^T = 0$ for no bulbous bow $K_{Tr}^T = 0.04$ for stern transom $K_{Tr}^T = 0$ for no stern transom  $K_{T1}^T = \frac{T_{ap} - T_{fp}}{T_{ap} + T_{fp}}$ where $T_{ap}$ is aft perp. static draft where $T_{fp}$ is fwd perp. static draft  $P_{Ch2} = 1$ for unrestricted channel $P_{Ch2} = 1 - 5S_h$ for restricted/canal
Barrass II (1979)	$S_{max} = \frac{C_B(A_s/A_w)^{2/3} V_k^{2.08}}{30}$ where $A_w$ is net cross section area of waterway $V_k$ is ship speed in knots
Führer & Römisch (1977)	$S_{max} = 8 \left[ \frac{V}{V_{crit,p}} \right]^2 \left[ \left( \frac{V}{V_{crit,p}} - 0.5 \right)^4 + 0.0625 \right] S_{crit}$  $V_{crit,p}$ is critical speed with self-propulsion effect: $V_{crit,p} = 0.92V_{crit}$ for $\frac{A_m}{A_c} \geq \frac{1}{6}$ $V_{crit,p} = 0.95V_{crit}$ for $\frac{1}{15} < \frac{A_m}{A_c} < \frac{1}{6}$ $V_{crit,p} = 1.00V_{crit}$ for $\frac{A_m}{A_c} \leq \frac{1}{15}$  If $L_{PP} \leq 3b$ & $A_m/A_c < 1/6$ $V_{crit} = \left[ \frac{hL_{PP}}{80TB} \right]^\beta \sqrt{gh}$ $\beta = 0.24 \left[ \frac{L_{PP}}{b} \right]^{0.55}$ where $b$ is channel waterline width  If $L_{PP} > 3b$ $V_{crit} = \left[ \frac{hL_{PP}}{80TB} \right]^{0.125} \sqrt{gh}$

	$S_{crit} = 0.2 \left[ \frac{10C_B B}{L_{PP}} \right]^2 T$ for bow squat $S_{crit} = 0.2T$ for stern squat
Hoof (1974)	$S_{bow} = \left( C_z + \frac{1}{2} C_\theta \right) \frac{\nabla}{L_{PP}^2} \frac{Fr_h^2}{\sqrt{1 - Fr_h^2}}$ $C_z = 1.46$ $C_\theta = 1.0$
Huuska (1976)	$S_{bow} = 2.4 \frac{\nabla}{L_{PP}^2} \frac{Fr_h^2}{\sqrt{1 - Fr_h^2}} K_s$  $K_s = 7.45s_1 + 0.76$ for $s_1 > 0.03$ $K_s = 1$ for $s_1 \leq 0.03$ $s_1 = (A_{s1}/A_c) + 0.76$ $K_1 =$ refer to Figure 10 $A_{s1} =$ midship section area $-0.98BT$
ICORELS (1980)	$S_{bow} = 2.4 \frac{\nabla}{L_{PP}^2} \frac{Fr_h^2}{\sqrt{1 - Fr_h^2}}$
Millward (1992)	$S_{mid} = \frac{38.0C_B T Fr_h^2}{100\sqrt{1 - Fr_h^2} L_{PP}}$ $S_{bow} = \left( \frac{61.7C_B T}{L_{PP}} - 0.6 \right) \frac{Fr_h^2}{\sqrt{1 - Fr_h^2}} \frac{L_{PP}}{100}$
Römisch (1989)	$S_{max} = C_V C_F K_{\Delta T} T$ $C_V = 8 \left( \frac{V}{V_{Cr}} \right)^2 \left[ \left( \frac{V}{V_{Cr}} - 0.5 \right)^4 + 0.0625 \right]$ $C_F = \left( \frac{10C_B B}{L_{PP}} \right)^2$ for bow squat $C_F = 1$ for stern squat $K_{\Delta T} = 0.155\sqrt{h/T}$  Unrestricted shallow water: $V_{Cr} = 0.58 \left( \frac{hL}{TB} \right)^{0.125} \sqrt{gh}$  Restricted channel: $V_{Cr} = \left[ K_{ch} \left( 1 - \frac{h_T}{h} \right) + K_c \frac{h_T}{h} \right] \sqrt{gh_{mT}}$ $K_{ch} = 0.58 \left( \frac{hL}{TB} \right)^{0.125}$ $h_{mT} = h - h_T (1 - h_m/h)$ where $h_m$ is mean water depth $h_T$ is trench height  Canal: $V_{Cr} = K_c \sqrt{gh}$ $K_c = 0.2306 \log \left( \frac{A_c}{A_s} \right) + 0.044$

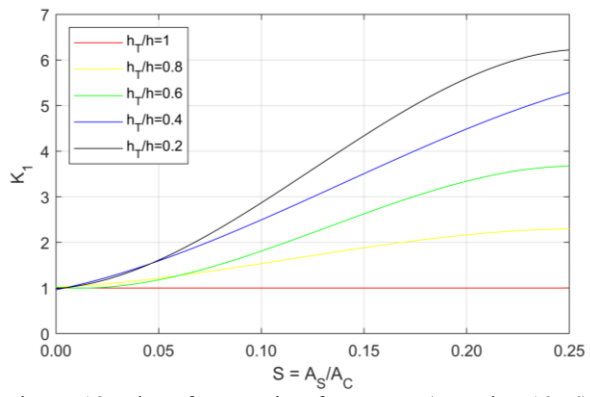


Figure 13: Plot of correction factor,  $K_1$  (Huuska, 1976).